

# A Numerical Investigation of Fracture Infilling and Spacing in Layered Rocks Subjected to Hydro-Mechanical Loading

L. C. Li · C. A. Tang · S. Y. Wang

Received: 5 August 2011 / Accepted: 10 October 2011  
© Springer-Verlag 2011

**Abstract** In order to better understand opening-mode fracture initiation and propagation perpendicular to the bedding plane at depth in sedimentary rocks, a series of two-dimensional (2D) numerical simulations is conducted. First, the stress states between two adjacent fractures for a typical three-layer model with pre-assigned fractures are simulated. Second, the same three-layer model without pre-assigned fractures is adopted to study the initiation and propagation of fractures in layered rocks. Numerical results show that infilling fractures grow more easily from flaws located near the interface than from those in the middle of the fractured layer. Flaws can begin to propagate to form a complete infilling fracture when the size of the flaws exceeds half of the thickness of the central layer. Under different overburden stress conditions and internal fluid pressure, the numerically obtained ratio of the critical fracture spacing to layer thickness varies between 0.465 and 0.833. This range encompasses the often-cited ratios of spacing to layer thickness in the literature for well-developed fracture sets. In addition, both the fracture pattern and the critical value of the fracture spacing to layer thickness ratio are strongly dependent on the heterogeneous characteristics of the central layer. In cases with a relatively homogeneous central layer, more interface fractures occur, and the interface delamination evidently influences the fracture saturation.

**Keywords** Numerical simulation · Hydro-mechanical behaviour · Fracture propagation · Damage · Heterogeneity · Rock

## 1 Introduction

Opening-mode fractures, or joints, are prevalent structural features of the earth's crust that occur in many different rock types and tectonic environments. These fractures commonly influence the movement and redistribution of fluids in most geologic environments and provide conditions for many sources of water, petroleum, and mineral deposits. Opening-mode fractures (joints) in layered sedimentary rocks are often confined by the layer boundaries, with their height being equal to their layer thickness (Helgeson and Aydin 1991; Gross and Engelder 1995). Many field observations suggest that joint spacing in layered sedimentary rocks is proportional to the thickness of the fractured layer, with the ratio of spacing to layer thickness ranging from  $<0.1$  to  $>10$  (Price 1966; Narr and Suppe 1991; Gross 1993; Gross and Engelder 1995; Wu and Pollard 1995; Becker and Gross 1996; Bai and Pollard 2000a, b; Bai et al. 2000; Jousineau and Petit 2007; Stefanizzi et al. 2007; Tang et al. 2008; Schöpfer et al. 2011). Based on frictional coupling between adjacent layers and the fractured layer, Kelly and Tyson (1965) and Price (1966) presented an important concept, called fracture saturation. Fracture saturation is closely related to fracture spacing. Wu and Pollard (1995) experimentally confirmed this concept. Using a three-layer elastic model with a fractured central layer and considering the interactions of Poisson's ratio, Bai and Pollard (2000a) demonstrated the existence of a critical spacing to layer thickness ratio for fracture development: when the ratio reaches a

---

L. C. Li (✉) · C. A. Tang  
School of Civil Engineering, Dalian University of Technology,  
Dalian 116024, People's Republic of China  
e-mail: li\_lianchong@163.com

S. Y. Wang  
Centre for Geotechnical and Materials Modelling, Civil,  
Surveying and Environmental Engineering, The University  
of Newcastle, Callaghan, NSW 2308, Australia

critical value ( $\sim 1.0$ ), normal stresses change from tensile to compressive. A change from tensile to compressive stress will halt the propagation of the fracture.

However, a preponderance of fracture data shows the spacing to layer thickness ratios to be less than the critical value (Laderia and Price 1981; Price and Cosgrove 1990). Bai and Pollard (2000b) called these types of fractures closely spaced fractures. The most prevalent explanations (Narr and Suppe 1991; Rives et al. 1992; Gross 1993; Becker and Gross 1996) for this phenomenon are variations of the concept proposed by Hobbs (1967). Later, joints are said to form in the intervals between the two adjacent joints formed earlier as a result of the stress transferred from adjacent layers, as the average strain increases. When the average strain reaches a certain value, either the tensile stress at the middle point achieves the level of the tensile strength of the rock, or the stress intensity factor of any flaw between the two earlier formed joints achieves the fracture toughness of the rock, and a new fracture forms.

Furthermore, the finite element method (FEM) and laboratory results summarised by Bai and Pollard (2000a) imply that with only an extension of the layers, it is impossible for new fractures to form between two earlier fractures if the spacing to layer thickness ratio of the earlier fractures is equal to or less than the critical ratio because the normal stress component in the direction perpendicular to the fractures is compressive. Therefore, different mechanisms must be considered to overcome the compressive stress. One possible mechanism is that the compressive stress between the two fractures is overcome by the local tensile stress produced where flaws (small cracks) exist in the fractured layer. Bai and Pollard (2000a) assumed that new fractures could form at depth in the crust under the action of overburden load and/or fluid pressure. In fact, in the earth's crust, many possible sources or mechanisms, including lithostatic forces, fluid pressure, tectonic forces, thermal energy, and other geological processes, such as magmatic intrusion or folding, can produce stresses that are strong enough to contribute to the formation of a new fracture (Engelder and Peacock 2001).

Previous studies on the relationship between joint spacing and bed thickness have examined cracks that have been subjected to far-field crack-normal tensile stress. Although absolute tensile stresses can occur under certain geological circumstances (e.g., above the neutral fibre in a buckle fold), the predominant state of stress in the brittle crust is triaxial or polyaxial compression. Many scholars believe that joint propagation is driven by fluids, whether by pore pressure changes (Secor 1965; Engelder and Lacazette 1990; Fischer et al. 1995; Sibson 1996; Bai and Pollard 2000a; Larsen et al. 2010) or by sub-critical crack growth following fluid-induced rock weakening (Savalli and Engelder 2005). The principal related work appears in

Pollard and Segall (1987) in which an analytical solution was found for the variation in crack-normal stress with distance  $x$  from the centre of the wall of a pressurised crack in a homogeneous, infinite elastic medium. To explain the formation of closely spaced fractures, Laderia and Price (1981) and Price and Cosgrove (1990) conceptually proposed that the joints in thick beds are produced by hydraulic fracturing.

Typically, hydraulic fracturing occurs when the fluid pressure in a flaw exceeds the least compressive stress by an amount necessary to raise the stress intensity at the crack tip to the fracture toughness of the rock. Fischer et al. (1995) investigated the stress distribution around the joints in layered rocks and found that the spacing of fluid-driven joints should depend on lithology and fluid pressure, at least for homogeneous fluid pressure distributions in joints that are under compression. Sibson (1996) illustrated the effects of ground stress on the permeability enhancement of rock mass in various tectonic settings, as shown in Fig. 1. The fluid-driven structure in the rock mass was subsequently regarded as “self-generated” by the infiltrating fluids.

In addition, Mandl (2005) reported that high fluid pressures play a key role in the generation of tension joints. According to Mandl (2005), there are two types of hydraulic fractures. One type, called an internal hydraulic fracture, occurs when the pore pressure inside the bed is uniformly raised to a level sufficient to fracture the rock. The other type is a hydraulic intrusion fracture that occurs when the bed is ruptured by the “wedging” action of highly pressurised fluid injected from outside. The two fracture types are schematically shown for horizontal layers in Fig. 2.

The mechanical explanation for this relationship is well understood when the joints are driven by far-field crack-normal tensile stresses, however, poorly understood for the origin and evolution of cracks driven by the difference between the crack-normal compression stress and the fluid pressure in the crack (Fischer et al. 1995). In most sedimentary basins, these conditions are dominant (Breckels and Eekelen 1982; Engelder and Fischer 1994). To better understand the origin and evolution of cracks driven by hydro-mechanical loading, we conducted a series of numerical simulations using the rock fracture process analysis (RFPA) code. Simulations modelled the progressive evolution of a fracture set during a controlled loading sequence and provided direct observations of the fracture initiation and progressive infilling behaviours. Unlike static stress analysis approaches in which the fractures have to be inserted into the model, our numerical code can model the complete fracture forming process. This fracture modelling technique can provide valuable insight concerning fracture processes that are impossible to observe in nature and

**Fig. 1** Schematic illustration of the inception of a fault-fracture structure as a consequence of pressured fluid infiltration into stressed heterogeneous crust (Sibson 1996)

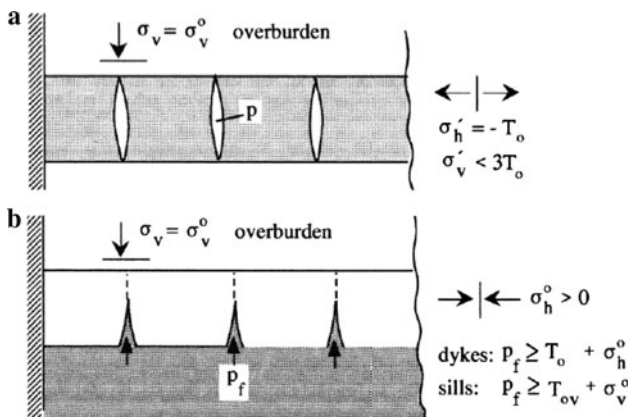
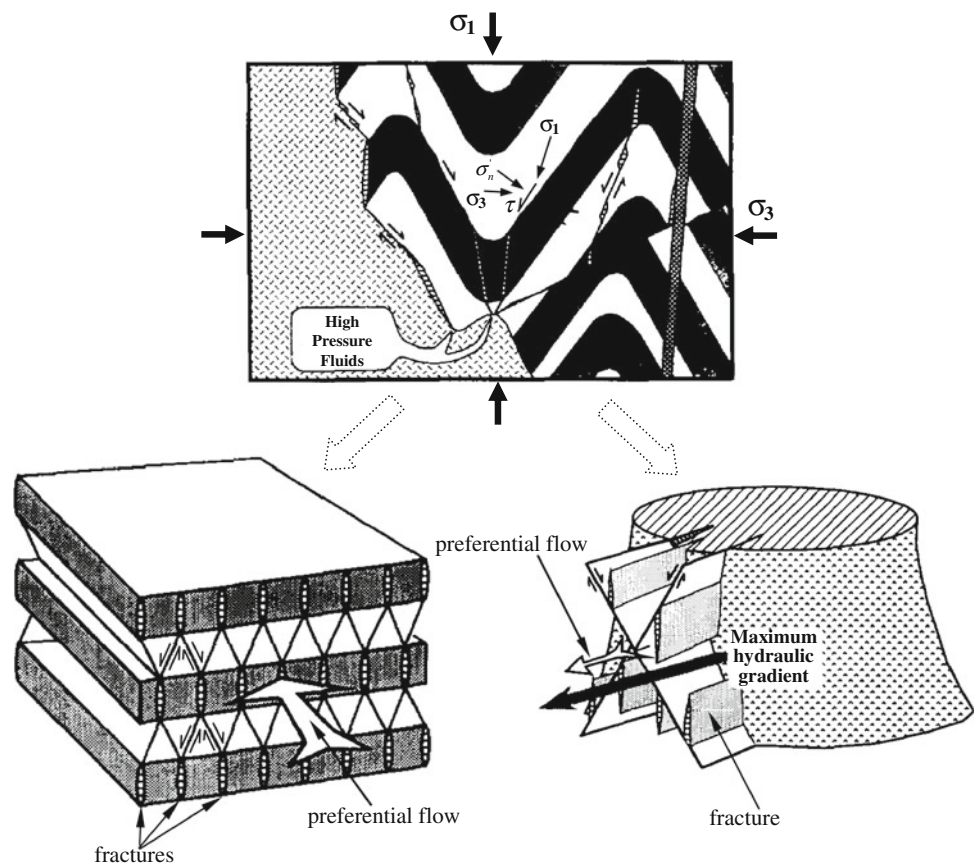


**Fig. 2** Hydraulic fractures: **a** internal fractures and **b** intrusion fractures (Mandl 2005)

difficult to consider using static stress analysis approaches. By changing the material heterogeneity of the model, we are able to examine how spacing is dependent on heterogeneity at each stage of development.

In this article, first, the stress states between two adjacent fractures for a typical three-layer model are numerically simulated. Second, the same three-layer model, except without pre-existing fractures, is applied to investigate the progressive evolution of a fracture subjected to

coupled hydro-mechanical loading. The term “fracture” in this article describes a planar discontinuity that shows predominantly opening-mode displacement and cuts through the fractured layer, i.e., it extends from one of the interfaces of the fractured layer to the other. The term “flaw” is used for a primarily opening-mode discontinuity that does not fully extend the thickness of the fractured layer. Fractures form by propagation of flaws or a coalescence of multiple flaws.

## 2 An Introduction to the Numerical Method

Briefly, RFPFA (Tang et al. 2002) represents a two-dimensional finite element code that can simulate the fracture and failure process of quasi-brittle materials, such as rock. To model the failure of rock material (or rock mass), the rock medium is assumed to be composed of many mesoscopic elements whose material properties are different from one another and are specified according to a Weibull distribution (Tang et al. 2000). The finite element method is employed to obtain the stress fields in the mesoscopic elements. Elastic damage mechanics is used to describe the constitutive law of the mesoscale elements. An element is considered to have failed in the tension mode when its

minor principal stress exceeds the tensile strength of the element (Eq. 1) and is considered to have failed in the shear mode when the shear stress satisfies the Mohr–Coulomb failure criterion (Eq. 2):

$$\sigma'_3 \leq -\sigma'_t, \quad (1)$$

where  $\sigma'_3$  is the minor effective principal stress, and  $\sigma'_t$  is the tensile failure strength of the element.

$$F = (c' + \sigma' \tan \phi') - \tau', \quad (2)$$

where  $\tau'$  is the effective shear stress,  $\sigma'$  is the effective normal stress,  $c'$  is the effective stress cohesion intercept, and  $\phi'$  is the internal friction angle of the elements (Tang and Kaiser 1998; Tang et al. 2000; Wong et al. 2006; Zhu et al. 2006; Wang et al. 2011).

For heterogeneous rock, the material properties, including the Young's modulus, Poisson's ratio and strength properties ( $\sigma'_t$ ,  $c'$ ,  $\phi'$ ), for different elements were randomly distributed throughout the domain of analysis following a Weibull distribution,

$$\phi = \frac{m}{\mu_0} \left( \frac{\mu}{\mu_0} \right)^{m-1} \exp \left[ - \left( \frac{\mu}{\mu_0} \right)^m \right], \quad (3)$$

where  $\mu$  is a material property variable, and  $\mu_0$  is the mean value of the corresponding material property. The homogeneity index  $m$  is a parameter defined by the shape of the distribution function that, in turn, defined the degree of material heterogeneity; a larger  $m$  implies a more homogeneous material, and vice versa. In general, it is assumed that Young's modulus and strength properties conform to two individual distributions with the same heterogeneity index. The distribution of Poisson's ratio is not notably dispersed in reality, and, therefore, a high homogeneity index of 100 is specified in the following simulations. Systematic studies of the homogeneity index  $m$  have been conducted previously (Tang et al. 2000; Wong et al. 2006; Zhu et al. 2006).

When rocks fail under applied loads, fissures or fractures form; therefore, the permeability of rock will undoubtedly increase dramatically. The failure of the rock results in a dramatic increase in permeability. During elastic deformation, the rock permeability decreases when the rock becomes compact and increases when the rock is extended or is under tension. However, the variation of permeability in these situations is limited. After reaching the strength point, dramatic increases in rock permeability can be expected, as a result of the generation of numerous fractures. In other words, the damage to the rock leads to a significant increase in the permeability. On reaching the strength value, the permeability drops again if the failed rock continues to be compacted, or the permeability

increases continuously if the failed rock is further extended. This extension constitutes a coupling relationship of seepage and damage (Tang et al. 2002).

Furthermore, for the coupling relationship of seepage and stress variations in saturated rock, Biot's theory of consolidation is adopted (Tang et al. 2002). The basic formulations of the analysis are

$$\text{Equilibrium equation : } \frac{\partial \sigma_{ij}}{\partial x_j} + \rho X_j = 0 \quad (i, j = 1, 2, 3) \quad (4)$$

$$\text{Geometrical equation : } \varepsilon_{ij} = \frac{1}{2}(u_{i,j} + u_{j,i}) \quad (5)$$

$$\varepsilon_v = \varepsilon_{11} + \varepsilon_{22} + \varepsilon_{33}$$

$$\text{Constitutive equation : } \sigma'_{ij} = \sigma_{ij} - \alpha p \delta_{ij} = \lambda \delta_{ij} \varepsilon_v + 2G \varepsilon_{ij} \quad (6)$$

$$\text{Seepage equation : } k \nabla^2 p = \frac{1}{Q} \frac{\partial p}{\partial t} - \alpha \frac{\partial \varepsilon_v}{\partial t} \quad (7)$$

$$\text{Coupling equation : } k(\sigma, p) = \zeta k_0 e^{-\beta \left( \frac{\sigma}{3} - \alpha p \right)}, \quad (8)$$

where  $\sigma_{ij}$  is total stress in the  $ij$ -plane,  $\rho$  is unit weight of rock matrix,  $X_j$  is body force in the  $j$ th direction,  $\varepsilon_{ij}$  is strain in the  $ij$ -plane,  $u_i$  the displacement in the  $i$ th direction,  $\sigma'_{ij}$  is the effective stress in the  $ij$ -plane,  $\alpha$  is coefficient of pore water pressure,  $p$  is pore water pressure,  $\lambda$  is Lamé coefficient,  $\delta_{ij}$  is Kronecker constant,  $G$  is modulus of shear deformation,  $k$  is the coefficient of permeability,  $Q$  is Biot's constant,  $\zeta$  is the permeability increase factor,  $\beta$  is the coupling coefficient, and  $\sigma_{ij}/3$  is the average stress. Equations 4 through 7 are derived from Biot's theory of consolidation. Equation 8 is introduced to describe the dependency of the permeability on stress and damage. Based on Biot's linear elastic constitutive theory, given a volume of fluid-filled rock subjected to an increase in confining compressive stress, the pore water pressure will increase if the pore fluid is prevented from flowing (i.e., if the stress state is undrained). Alternatively, if the pore water pressure is increased or decreased, then the effective stress on the volume of rock will change accordingly. Depending on the boundary conditions applied to the model, these changes in pore pressure may induce rock deformation (Yang et al. 2004; Tham et al. 2005; Wang et al. 2009).

In addition, in RFPA<sup>2D</sup>, because a failed element must release the elastic energy stored during deformation, the failure (or damage) of each element is assumed to represent the source of an acoustic event (Tang et al. 2002). Therefore, by recording the number of damaged elements and the associated amounts of energy release, RFPA<sup>2D</sup> is capable of simulating acoustic emission (AE) activity, including the AE event rate, the magnitudes of microseismic events and

their locations. In the numerical simulations of rock failure, the AE distributions of some specimens are also used to indicate the locations of fracture initiation and the paths of propagation during the failure process. For a detailed introduction to the models and verifications, see previous numerical simulations (Tang and Kaiser 1998; Tang et al. 2002; Yang et al. 2004; Tham et al. 2005).

### 3 Numerical Modelling

#### 3.1 Stress Distribution between Adjacent Fractures

The following analyses have been performed to study fracturing behaviour in multiple-layer rocks. Before reporting the results of our simulations in progressive fracture modellings, we focus on the stress distribution that governs the model's fracturing behaviour. We use a three-layer model discretised into a mesh that contains  $600 \times 150 = 90,000$  elements with geometry of  $2,000 \times 500$  mm. The thickness of the central layer ( $T_c$ ) is 100 mm. The overall thickness of the model ( $T$ ) is 500 mm, which can be defined as  $T = T_c + T_b + T_t$ , as shown in Fig. 3. The Young's modulus ( $E_b$ ), compressive strength ( $\sigma_b$ ), and Poisson's ratio ( $\nu_b$ ) are the same for adjacent layers ( $E_b = 15$  GPa,  $\sigma_b = 300$  MPa,  $\nu_b = 0.35$ ), and the values for the central layer are 50 GPa, 100 MPa, and 0.25, respectively. A compressive vertical stress ( $\sigma_v$ ) of 15.0 MPa is imposed on the top boundary, and a horizontal stress ( $\sigma_h$ ) of 7.5 MPa is imposed on the right- and left-side boundaries. Normal displacements are constrained on the bottom boundary. Plane strain is assumed for all calculations. The objective of this section is to investigate the stress distribution in the model with hypothetically pre-assigned fractures; therefore, a uniform pore pressure of 15.0 MPa is imposed throughout the interior area of the model. Boundary conditions imposed on the model include impermeable top and bottom boundaries and 0 MPa pore pressure on the left and right permeable boundaries.

Four fractures are pre-assigned in the central layer, and they are equally spaced along the central layer and

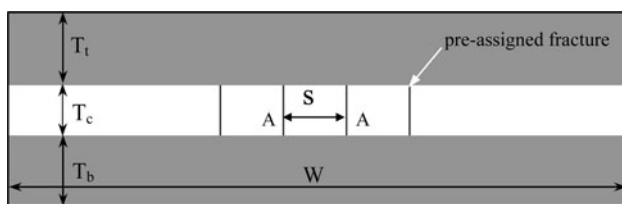


**Fig. 3** The configuration of a three-layered model. The thickness of the central layer and the neighbouring layers are indicated by  $T_c$ ,  $T_t$ , and  $T_b$ , respectively. The space of the adjacent fractures is denoted by  $S$ , and the entire width is denoted by  $W$

perpendicular to the long axis and fully transect the layer height ( $T_c$ ). With this defined model, the evolution of the stress distribution is examined as a function of the fracture spacing to the fractured layer thickness ratio. To clearly understand the transition of stress along the line A–A in Fig. 3 for a homogeneous medium, the homogeneity index is set to represent a uniform material, with  $m$  being large enough to represent a homogeneous material.

From Fig. 4, the minimum principal stress ( $\sigma_3$ ) distribution in the central layer has an obvious transition from tensile to compressive. To perform a quantitative analysis, we use the stress along the line A–A to represent the stress between adjacent fractures. The stress distribution shown in Fig. 5 indicates that the critical spacing to fractured layer thickness ratio is approximately 0.6. This critical value determines the stress state between the adjacent fractures: when the ratio is below this critical value, the stress along line A–A is compressive, and when it is above the critical value, the stress is tensile. In the study, the loading pattern is different from those used in previous studies, and the deformation of the central layer is controlled by both internal fluid pressure and the effect of contrasts in elastic properties between layers. Therefore, the critical spacing to fractured layer thickness ratio obtained in this study is lower than 1.0. The stress state transition implies that a new fracture cannot fill in between two fractures with a spacing to layer thickness ratio less than the critical value unless a flaw exists in the middle of the fractured layer, thereby cutting through the compressive region. Another possible exception is that a flaw near one of the interfaces propagates toward the other interface and cuts through the region of compressive stress. The following numerical results regarding the fracture pattern for heterogeneous materials show that during the process of fracture infilling, the new fracture does not always initiate at the middle point between the earlier formed fractures. Instead, the new fracture initiates at a point where the local element stress reaches its failure strength.

#### 3.2 The Fracture Infilling Process

In the previous section, we confirmed that a stress-state transition existed between two adjacent opening-mode fractures in a layered model. In this section, RFPA is used to model the fracture pattern of the same three-layer model but without pre-assigned fractures, as shown in Fig. 6. In this model, the homogeneity index  $m$  of the central layer is chosen to be 3.0. A uniform fluid pressure is applied to the whole model. The rate of pressurisation is maintained at a constant value throughout the numerical modelling at 0.1 MPa/step. This fracture modelling provides a unique opportunity to investigate the mechanism of how a fracture set evolves with coupled hydro-mechanical loading.

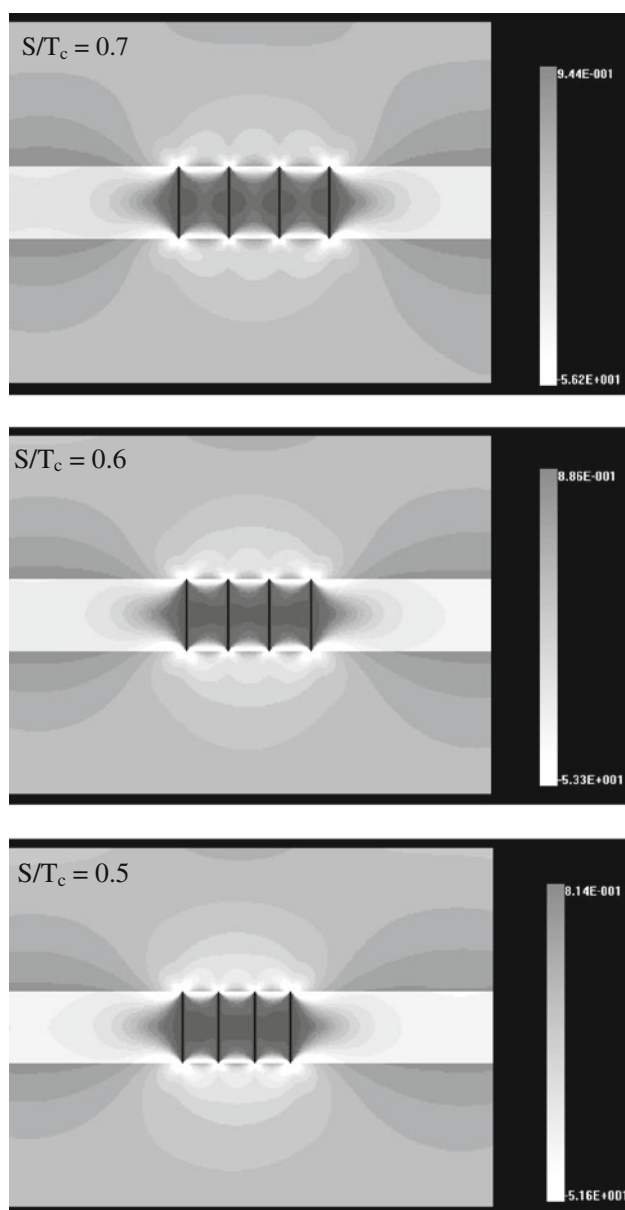


**Fig. 4** Distribution of stress  $\sigma_3$  in models with different fracture spacing to layer thickness ratios  $S/T_c$ . The different shades of grey represent different values of stress

Figure 7 illustrates the numerically obtained fracture infilling process and fracture saturation. According to the order of the fracture formation, we can divide the process into three stages. In the first stage (Fig. 7a, b), before the fluid pressure reaches 6.0 MPa, randomly distributed short fractures (flaws) form in the central layer at the weakest elements, where the local tensile stress reaches the local tensile strength. The initial fractures are isolated from these seed locations and do not interact. During this stage, the tensile stress results mainly from the local pore pressure and the contrasts in elastic properties of the involved stratigraphy. In the second stage (Fig. 7c–e), before the fluid

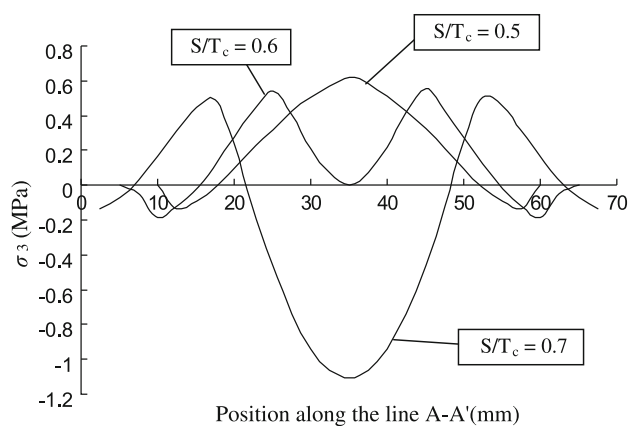


**Fig. 5** The stress variation along the line A–A between adjacent fractures as the fracture spacing to layer thickness ratio  $S/T_c$  decreases. The negative sign represents tensile stress, and the positive sign represents compressive stress. The figure indicates that 0.6 is the critical spacing to layer thickness ratio for stress transition from tension to compression

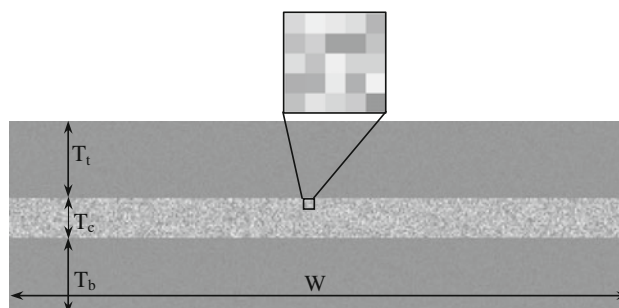


**Fig. 6** The configuration of a three-layer model without pre-assigned fractures. The inset shows in detail the heterogeneity in the model. Because the model has 90,000 elements, and the scale of the elements is too small to identify the element mesh, we show a small portion of the model in a large box. The different grey shades in the box represent different values of the mechanical properties of the individual elements

pressure reaches 7.5 MPa, nine long fractures sequentially penetrate through the central layer. It is noted that the strong interaction between the isolated fractures in this high-stress field makes the fractures propagate in an unstable manner. The variation in fracture mode is highly sensitive to the local disordered feature of the rock. As a result, the fracture surface is not straight, but flexural and rough.

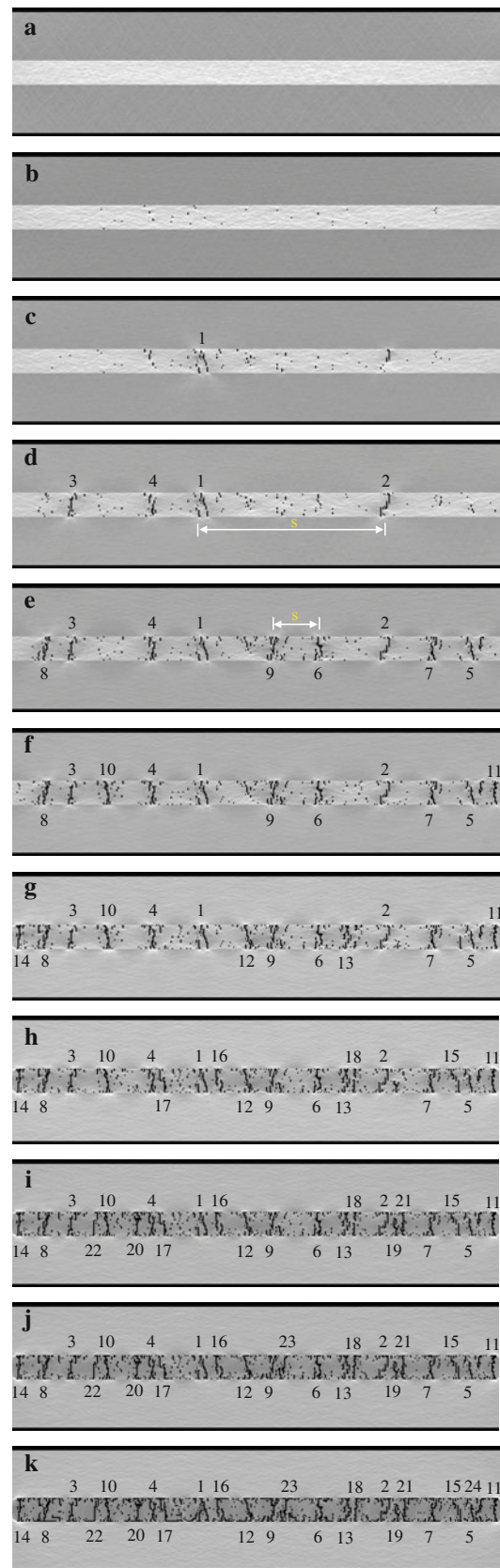
In reality, there are two types of failure for different materials: high-stress failure and low-strength failure. In a homogeneous material, failure begins at the high-stress site, whereas in heterogeneous material, e.g., rock, failure may start at the weaker locations because of the presence of features such as pores, micro-fractures, and grain boundaries. This property explains why Fairhurst (1964) introduced the notion of “stress severity”, which represents the ratio of the theoretical stress at the moment of failure to the

**Fig. 7** The infilling process of fractures simulated with RFPA<sup>2D</sup>. The numbers from 1 to 24 indicate the sequence of fracture infilling. The darker elements represent the nucleated flaws. Fractures form by the connection of flaws. The intensity of the shading indicates the relative magnitude of the maximum tension stress within the elements. This figure shows how the evolution of fracturing in the model affects the stress distribution

stress that would theoretically be necessary for failure at any given point. Heterogeneity is the main explanation for the failure that occurs in locations in which the stress is not necessarily the greatest. In the third stage (Fig. 7f–k), 15 additional fractures nucleate and infill between these first 9 fractures. Bai and Pollard (2000b) found that, in the case of pure extension and where fractures reached saturation, fractures are more likely to form near the interfaces than in the middle of the fractured layer. In our modelling, the common phenomenon, delamination or decohesion, is also commonly observed. Many fractures nucleate and propagate along the top and bottom interfaces of the central layer. Although the mechanisms of delamination have been discussed by several authors, such as He and Hutchinson (1989), Thouless (1989), Cherepanov (1994), and Bai et al. (2000), our direct fracture modelling approach demonstrated how delamination would affect the fracture saturation behaviour and the associated critical value of the spacing of fractures to the thickness of the fractured layer.

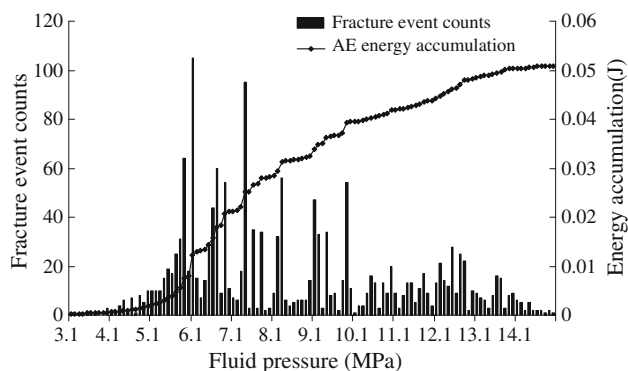
During the fracture infilling process, the top and bottom layers apply a local traction at all points to the central embedded layer, which has a non-zero shear modulus. Although the interface between layers is assumed to be perfectly bonded, numerical simulations show that the interface may not remain perfectly bonded at points of large strains, and delamination may occur if the shear stress near the layer boundary is sufficiently high. This delamination could significantly change the local stress state. One of the most important effects is that the interface delamination and through-going fracturing (fracture nucleation and propagation along the interface between layers) reduce the stress concentration induced by the contrasts in elastic properties between layers. In other words, the delamination will stop the transfer of stress from the neighbouring layers to the central layer and, in turn, prevent further infilling of new fractures between existing fractures in the central layer. This effect will result in a longer length scale of fracture spacing and will make the critical spacing to layer thickness ratio much greater. From the results of the numerical simulation of the model, we find that the number of fractures remains at 24 in the condition of saturation, and the critical spacing to fractured layer thickness ratio is about 0.8.

Figure 8 shows the temporal distribution of fracture events and AE (acoustic emission) energy release that



occurred during the loading process. The curve correlates well the fracture event counts, and the energy release rate correlates well with the fracture infilling phenomenon. In stage I, a steadily increasing number of small fractures with lower strength flaws propagate earlier because of their lower critical fracture stresses. However, in stage II, the number of flaw nucleation events no longer increases systematically with increasing fluid pressure. When a new fracture that cuts across the central layer forms, the fracturing process is accompanied by a rapid increase in the number of fracture events and an elevated rate of energy release. Once a thickness cut-through fracture nucleates, the layer generally remains stable during gradual increases in fluid pressure until critical local tensile stress is achieved between adjacent fractures. While in the saturation state, the magnitude of fracture events is also small, and the AE energy accumulation tends towards calm. A comparison between Figs. 7 and 8 reveals that each abrupt increase in the number of fracture events corresponds to an event of fracture infilling.

Another advantage of numerical simulation is that detailed information about stress distribution during the fracturing process can be obtained, including data on failure-induced stress redistribution. Figure 9 illustrates the variation in tensile stresses across section B–B in different loading stages. The figure shows that although the stress distribution at the initial loading stage is statistically homogeneous on a macroscale, it varies on a microscale because of the microscale heterogeneity of the model. Because of the fracture initiation, propagation, and coalescence, a high-stress concentration is induced. When large fracture zones develop, highly non-uniform stress distributions also develop, especially when the fracture zone is not immediately stress-free. With the increase in fluid pressure, stress distribution gradually becomes smooth on a macroscale, which also indicates that both the fractures in the central layer and the interface fractures between the adjacent layers are well developed.



**Fig. 8** Fracture-event counts and AE-released energy accumulation versus hydro-mechanical loading

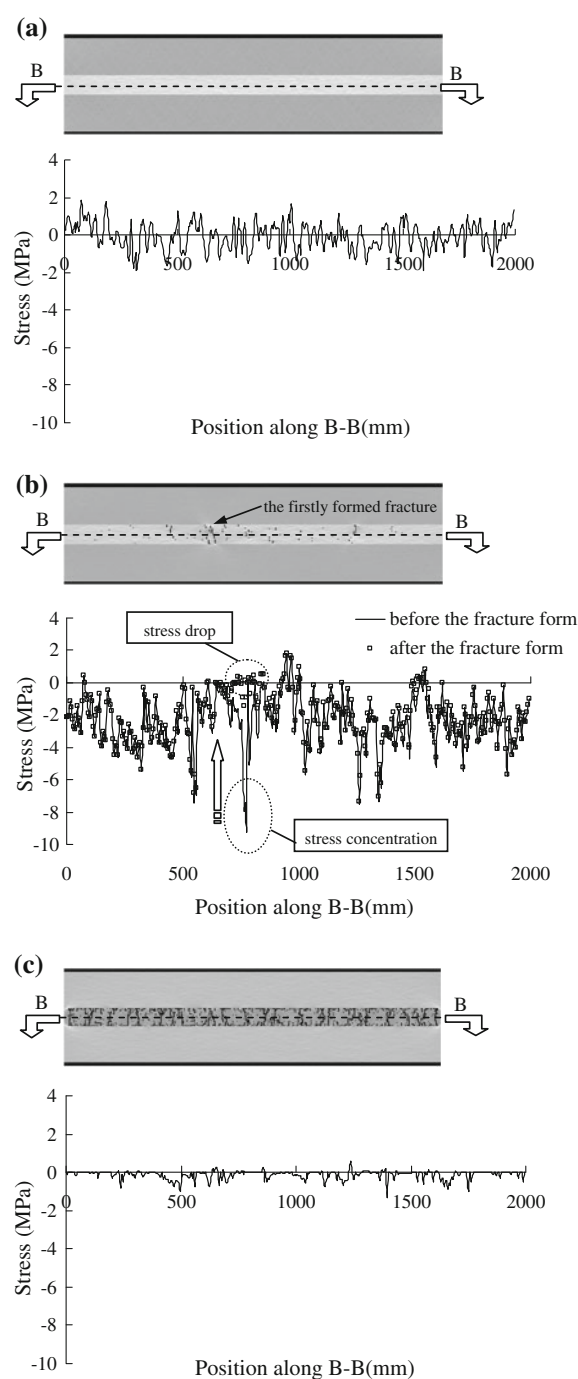
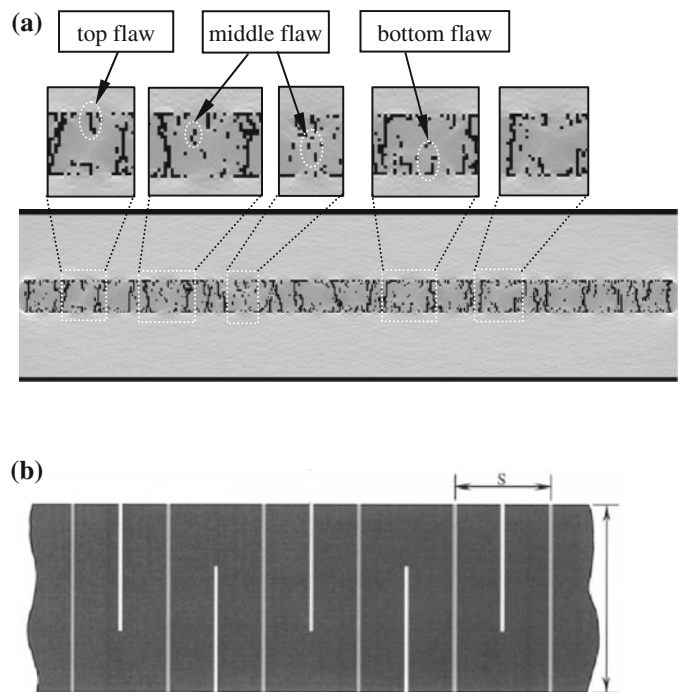


**Fig. 9** Stress distribution and failure-induced stress redistribution along the line B–B across the fractured layer. At a lower stress level, the stress fluctuation is influenced mainly by the microscale heterogeneity of the model. At a higher stress level, the stress fluctuation is influenced mainly by the newly formed fracture propagation. Once the fractures are completely developed, the stress distribution gradually becomes uniform and smooth on a macroscale. The *negative sign* represents the tensile stress, and the *positive sign* represents the compressive stress. **a** Stress distribution when the internal fluid pressure is 4.0 MPa. **b** Stress distribution when the internal fluid pressure is 6.0 MPa. **c** Stress distribution when the internal fluid pressure is 15.0 MPa

**Fig. 10** Overview of partially infilling cracks. **a** Numerically obtained partially infilling cracks. **b** Physical views of partially infilling cracks presented by Bai and Pollard (2000b)



### 3.3 Propagation of Partially Infilling Cracks and Complete Infilling

In the above numerical calculations the spacing to layer thickness ratio (0.8) considered in the model for specific loading and boundary conditions is greater than the critical value (0.6) obtained from the stress analysis in Sect. 3.1. One explanation for this difference is delamination or decohesion, and another is the emergence of partially infilling cracks (flaws). Figure 10a shows the partially amplified fracture spacing of the numerical results in Sect. 3.2. In Fig. 10a, we can clearly observe the partially infilling cracks. Figure 10b shows the partially infilling cracks presented by Bai and Pollard (2000b). Although many scholars (Narr and Suppe 1991; Rives et al. 1992; Gross 1993; Becker and Gross 1996; Bai and Pollard 2000b) have discussed how such flaws might be initiated, our direct fracture modelling distinctly demonstrated the initiation of a flaw and the critical value of the spacing of fractures associated with the thickness of the fractured layer.

Figure 10a shows that the configuration of flaws has three distinct characteristics. The first characteristic is that most of the flaws initiate from the interfaces rather than from the central part of the central layer. The second characteristic is that the flaws (i.e., the top flaw and the bottom flaw) located near the interfaces are relatively longer than those (e.g., the middle flaws) located in the central part of the central layer. The third characteristic is that the size of most of the flaws that initiated from the

interfaces is less than half of the thickness of the central layer. These results imply that with all other parameters being equal, the top and bottom flaws are more likely to propagate, and the middle flaws of this size near the central part are unlikely to propagate. The top and bottom flaws could begin to propagate to form a complete infilling fracture as soon as the size of the flaws exceeds half of the thickness of the central layer.

How might such flaws be propagated to form a complete infilling fracture? Although Bai et al. (2000) did not conduct an analysis of fracture controlled by the fluid pressure, they concluded that the sequential infilling by crack-like flaws between existing fractures, if such flaws exist, could occur at depth in the earth's crust under the action of overburden load and/or fluid pressure. Therefore, mechanisms other than pure extension (i.e., overburden load and/or internal fluid pressure) are apparently required to explain the propagation of the partially infilling cracks.

To investigate the fracturing process of partially infilling cracks, while keeping all other boundary conditions identical (Fig. 6), five models with different values of overburden load ( $\sigma_v = 15.0, 18.75, 20.0, 22.5$  and  $25.0$  MPa) are used. The fluid pressure is applied to the whole model. The rate of pressurisation is kept constant throughout the numerical tests at 0.1 MPa/step.

Figure 11 shows the numerically obtained fracture spacing at the final loading stage. All the simulations produce a similar relationship between spacing and thickness: spacing decreases rapidly at first, before slowing down and approaching a nearly constant value. Comparing

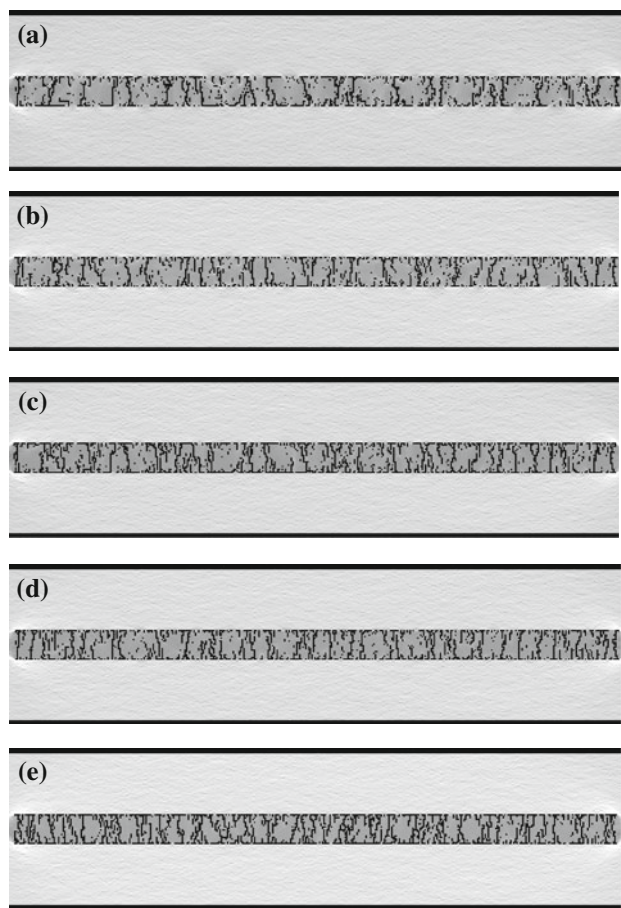


**Fig. 11** Fracture pattern for the five models with different overburden stresses. **a**  $\sigma_v = 15.00$  MPa ( $S/Tc = 0.8$ ), **b**  $\sigma_v = 18.75$  MPa ( $S/Tc = 0.714$ ), **c**  $\sigma_v = 20.00$  MPa ( $S/Tc = 0.606$ ), **d**  $\sigma_v = 22.50$  MPa ( $S/Tc = 0.556$ ), **e**  $\sigma_v = 25.00$  MPa ( $S/Tc = 0.465$ )

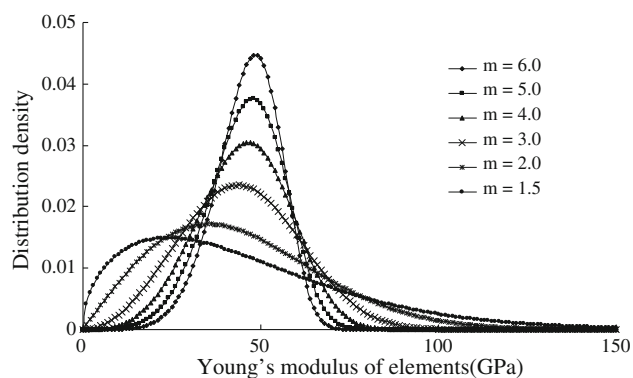


**Fig. 12** Stochastic distribution of Young's modulus of elements with different homogeneity indexes,  $m$ . The strength of elements follows the same distribution

our numerical results from the five models, the critical ratio for saturation spacing is found to decrease systematically from 0.8 to 0.465. One explanation for this decrease is that with the increase in the compressive overburden stress, the tensile strength of the rock between the joints is enhanced

accordingly. Also, the number of infill fractures (tensile fractures) is reduced accordingly. Another explanation is that the interfacial debonding becomes more difficult when the interfacial normal stress increases because of the increasing compressive overburden stress. This range of critical values between 0.8 and 0.465 encompasses the often-cited spacing to layer thickness ratios in the literature for well-developed fracture sets (Bai et al. 2000).

### 3.4 Effects of the Heterogeneity on the Fracture Spacing to Layer Thickness Ratio

To study the influence of heterogeneity on the fracture patterns and the critical fracture spacing to layer thickness ratio, we chose six different values of the homogeneity index of the central layer,  $m = 1.5, 2.0, 3.0, 4.0, 5.0,$  and  $6.0$ . This range of values for the homogeneity index represents relatively heterogeneous to relatively homogeneous materials. All of the other boundary conditions are the same as before (Fig. 6). Figure 12 shows the shape of the probability density function with the homogeneity index  $m$ . Figure 13 shows the corresponding numerical models with different homogeneity indexes. In this figure, the different shades of grey correspond to different magnitudes of Young's modulus of elements. It can be observed that the Young's modulus of elements is more concentrated and closer to 50 GPa with the increase of the homogeneity index  $m$ . Therefore, the increase of the homogeneity index leads to a more homogeneous numerical model.

The final stage of the modelling for all six models is presented in Fig. 13. It is found that fractures did not form through the crack propagation for the highly heterogeneous material model but rather formed through the coalescence of the independent cracks. However, the fractures tended to form through the propagation of newly nucleated small cracks in lines that are more or less perpendicular to the layer. With the influence of the heterogeneity of the material, new fractures are observed to form at locations that are not always between the adjacent fractures that were formed earlier. The failure modes are sensitive to the local disorder feature of the central layer material. The fracture path of a homogeneous case is smoother than that of a heterogeneous case. The fracture propagation follows a more or less wavy path across the layer. In addition, the fracture nucleation sometimes starts from the interface rather than from the interior of the layer.

Although the fracturing pattern is complex with the influence of heterogeneity, the length scale of fracture spacing shows an overall scaling behaviour that is closely related to the behaviour of homogeneous materials. However, a quantitative difference in length scale of fracture

**Fig. 13** Fracture patterns at saturation for the six models with different homogeneity indexes,  $m = 1.5, 2.0, 3.0, 4.0, 5.0,$  and  $6.0$ . It is shown that the number of vertical fractures in the central layer decreases, and on the whole, more interface fractures occur with increasing homogeneity index

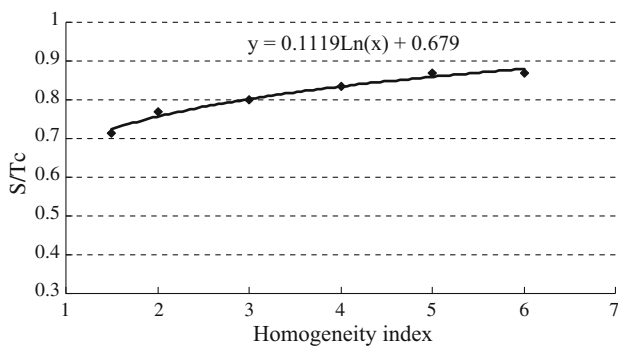
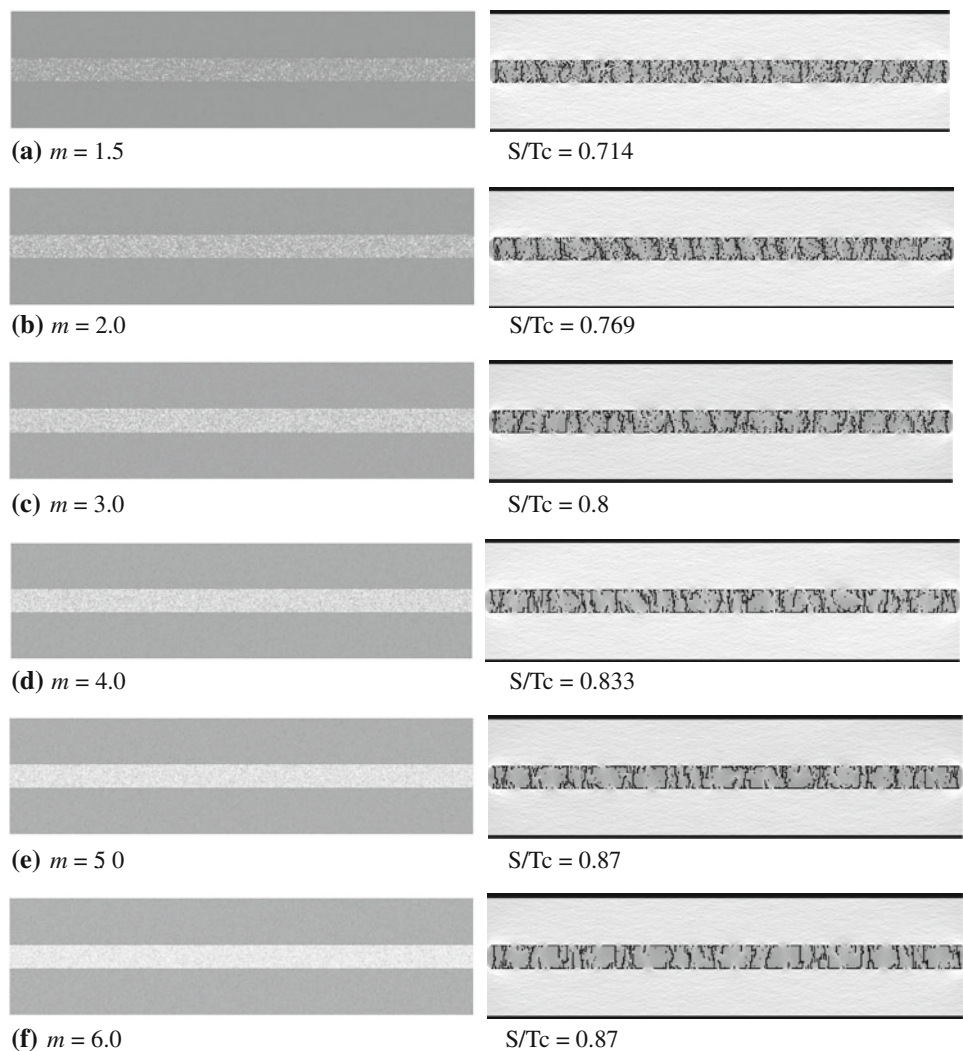


**Fig. 14** Numerically obtained critical ratio of fracture spacing to layer thickness as a function of homogeneity index

spacing is found between the heterogeneous and homogeneous models. The critical spacing to layer thickness ratio is nonlinearly related to the homogeneity index, as shown in Fig. 14. Although the critical fracture spacing to layer thickness ratios for all of the cases are lower than 1.0, the ratio increases with increasing homogeneity index.

Increasing heterogeneity of the layer increases the variation magnitude of the local stress concentration, which results in more fractures forming in a lower stress level. For a relatively heterogeneous case, the fractures reach the saturation state before interface delamination occurs. At a higher stress level, interface cracks begin to form, and delamination begins to occur. Delamination can significantly change the local stress state.

#### 4 Conclusions

In this study, the RFPA<sup>2D</sup> code was applied to simulate the stress state and evolution of opening-mode fractures in multi-layer rocks that were subjected to coupled hydro-mechanical loading. Although practical cases are often much more complex than the numerical models considered, the study highlights some interesting phenomena for elucidating the failure mechanisms of layered rocks. Based on numerical results, the conclusions are the following:

1. Layered rocks can contain well-developed sets of opening-mode fractures with spacing that is equal to or smaller than the height of the fractured layers, even in fractures that are relatively dense and at great depth. This is because several possible mechanisms that are capable of producing high stresses in the earth's crust, including pressurised fluid, tectonic forces, thermal energy, and other geological processes, may help keep the fractures open at depth. Most of the infilling fractures, which developed from a flaw with one of its tips located at the interface, can cut through the fractured layer (complete infilling) only if the crack propagates beyond the middle line of the central layer. Otherwise, the infilling fracture can only partially cut the fracture layer (partial infilling) because the maximum compressive stresses are located at the central point between the existing complete infilling fractures. However, overburden load and/or internal fluid pressure can overcome this compressive stress.
2. During the infilling process, the newly formed fractures and the crack-like flaws between existing fractures directly govern the stress redistribution. The compressive overburden stress in the direction parallel to the fractures could produce tensile stress in the direction perpendicular to the fractures. The magnitude of this tensile stress increases with internal fluid pressure in the flaw. With a specific overburden stress and internal fluid pressure, the flaws of specific sizes can significantly change the local stress field, that is, a crack can propagate into and through the compressive stress region. When large fracture zones develop at relatively elevated stress levels, highly non-uniform stress distributions develop, especially when the fracture zone is not immediately stress-free. As the fractures become well developed, the stress distribution becomes uniform and smooth on a macro-scale.
3. Heterogeneity is a key factor that influences the fracture pattern in modelling. For the case with a highly heterogeneous property of the central layer, the path of the infilling fractures is irregular, and the location is isolated, whereas in the more homogeneous case, the fracturing path is relatively smooth, and the location is more symmetrical. Although the critical fracture spacing to layer thickness ratios for all of the cases are below 1.0, the ratio increases with an increasing homogeneity index. This result is observed because the interface delamination stopped the transition of stress from the neighbouring layers to the central layer. As a result, the tensile stress between the adjacent existing fractures is not large

enough to provide the power for the flaws to initiate and propagate.

**Acknowledgments** The study presented in this article was jointly supported by grants from the China National Natural Science Foundation (grant no. 50909013), the National Basic Research Programme of China (grant no. 2011CB013503), and the Specialized Research Fund for the Doctoral Programme of Higher Education (SRFDP) of China (grant no. 20090041120024). ARC Australian Laureate Fellowship grant FL0992039.

## References

- Bai T, Pollard DD (2000a) Fracture spacing in layered rocks: a new explanation based on the stress transition. *J Struct Geol* 22:43–57
- Bai T, Pollard DD (2000b) Closely spaced fractures in layered rocks: initiation mechanism and propagation kinematics. *J Struct Geol* 22:1409–1425
- Bai T, Pollard DD, Gao H (2000) Explanation for fracture spacing in layered materials. *Nature* 403:753–756
- Becker A, Gross MR (1996) Mechanism for joint saturation in mechanically layered rocks: an example from southern Israel. *Tectonophysics* 257:223–237
- Breckels IM, Eekelen HAMV (1982) Relationship between horizontal stress and depth in sedimentary basins. *J Pet Technol* 34:2191–2199
- Cherepanov GP (1994) On the theory of thermal stresses in a thin film on a ceramic substrate. *J Appl Phys* 75:844–849
- Engelder T, Fischer MP (1994) Influence of poroelastic behavior on the magnitude of minimum horizontal stress,  $S_h$ , in overpressured parts of sedimentary basins. *Geology* 22:949–952
- Engelder T, Lacazette A (1990) Natural hydraulic fracturing. In: *Proceeding of international symposium on rock joints*. Loen, Norway, pp 35–43
- Engelder T, Peacock DCP (2001) Joint development normal to regional compression during flexural-flow folding: the Lilstock buttress anticline, Somerset, England. *J Struct Geol* 23:259–277
- Fairhurst C (1964) On the validity of the Brazilian test for brittle materials. *Int J Rock Mech Min Sci* 1:535–546
- Fischer MP, Gross MR, Engelder T, Greenfield RJ (1995) Finite-element analysis of the stress distribution around a pressurized crack in a layered elastic medium: implications for the spacing of fluid driven joints in bedded sedimentary rock. *Tectonophysics* 247:49–64
- Gross MR (1993) The origin and spacing of cross joints: examples from Monterey Formation, Santa Barbara coastline, California. *J Struct Geol* 15:737–751
- Gross MR, Engelder T (1995) Strain accommodated by brittle failure in adjacent units of the Monterey Formation, U.S.A.: scale effects and evidence for uniform displacement boundary conditions. *J Struct Geol* 17:1303–1318
- He MY, Hutchinson JW (1989) Kinking of a crack out of an interface. *J Appl Mech* 56:270–278
- Helgeson DE, Aydin A (1991) Characteristics of joint propagation across layer interfaces in sedimentary rocks. *J Struct Geol* 13:897–911
- Hobbs DW (1967) The formation of tension joints in sedimentary rocks: an explanation. *Geol Mag* 104:550–556
- Joussineau Gd, Petit JP (2007) Can tensile stress develop in fractured multilayers under compressive strain conditions. *Tectonophysics* 432:51–62

- Kelly A, Tyson WR (1965) Tensile properties of fiber-reinforced metals: copper/tungsten and copper/molybdenum. *J Mech Phys Solids* 13:329–350
- Laderia FL, Price NJ (1981) Relationship between fracture spacing and bed thickness. *J Struct Geol* 3:179–183
- Larsen B, Grunnaleite I, Gudmundsson A (2010) How fracture systems affect permeability development in shallow-water carbonate rocks: an example from the Gargano Peninsula, Italy. *J Struct Geol* 32:1212–1230
- Mandl G (2005) Rock joints. The mechanical genesis. Springer, Heidelberg, pp 27–48
- Narr W, Suppe J (1991) Joint spacing in sedimentary rocks. *J Struct Geol* 13:1037–1048
- Pollard DD, Segall P (1987) Theoretical displacements and stresses near fracture in rock: with applications to faults, joints, veins, dikes, and solution surfaces. In: Atkinson BK (ed) *Fracture mechanics of rock*. Academic Press, London, pp 277–349
- Price NJ (1966) Fault and joint development in brittle and semi-brittle rocks. Pergamon Press, Oxford
- Price NJ, Cosgrove JW (1990) *Analysis of geologic structures*. Cambridge University Press, Cambridge
- Rives T, Razack M, Petti JP, Rawnsley KD (1992) Joint spacing: analogue and numerical simulations. *J Struct Geol* 14:925–937
- Savalli L, Engelder T (2005) Mechanisms controlling rupture shape during subcritical growth of joints in layered rocks. *Geol Soc Am Bull* 117:436–449
- Schöpfer MPJ, Arslan A, Walsh JJ, Childs C (2011) Reconciliation of contrasting theories for fracture spacing in layered rocks. *J Struct Geol* 33:551–565
- Secor DT (1965) Role of fluid pressure in jointing. *Am J Sci* 263:633–646
- Sibson RH (1996) Structural permeability of fluid-driven fault-fracture meshes. *J Struct Geol* 18:1031–1042
- Stefanizzi S, Barla G, Kaiser PK (2007) Numerical modelling of strain-driven fractures around tunnel in layered rock masses. Euro Tun Congress, Vienna
- Tang CA, Kaiser PK (1998) Numerical simulation of cumulative damage and seismic energy release during brittle rock failure—Part I: fundamentals. *Int J Rock Mech Min Sci* 35:113–121
- Tang CA, Liu H, Lee PKK, Tsui Y, Tham LG (2000) Numerical studies of the influence of microstructure on rock failure in uniaxial compression—Part I: effect of heterogeneity. *Int J Rock Mech Min Sci* 37:555–569
- Tang CA, Tham LG, Lee PKK, Yang TH, Li LC (2002) Coupling analysis of flow, stress and damage (FSD) in rock failure. *Int J Rock Mech Min Sci* 39:477–489
- Tang CA, Liang ZZ, Zhang YB, Chang X, Xu T, Wang DG, Zhang JX, Liu JS, Zhu WC, Elsworth D (2008) Fracture spacing in layered materials: a new explanation based on two-dimensional failure process modeling. *Am J Sci* 308:49–72
- Tham LG, Liu H, Tang CA, Lee PKK, Tsui Y (2005) On tension failure of 2D rock specimens and associated acoustic emission. *Rock Mech Rock Eng* 38:1–19
- Thouless MD (1989) Some mechanics for the adhesion of thin films. *Thin Solid Films* 181:397–406
- Wang SY, Sun L, Au ASK, Yang TH, Tang CA (2009) 2D-numerical analysis of hydraulic fracturing in heterogeneous geo-materials. *Constr Build Mater* 23(6):2196–2206
- Wang SY, Sloan SW, Huang ML, Tang CA (2011) Numerical study of failure mechanism of serial and parallel rock pillars. *Rock Mech Rock Eng* 44(2):179–198
- Wong TF, Wong RHC, Chau KT, Tang CA (2006) Microcrack statistics, Weibull distribution and micromechanical modeling of compressive failure in rock. *Mech Mater* 38:664–681
- Wu H, Pollard DD (1995) An experimental study of the relationship between joint spacing and layer thickness. *J Struct Geol* 17:887–905
- Yang TH, Tham LG, Tang CA, Liang ZZ, Tsui Y (2004) Influence of heterogeneity of mechanical properties on hydraulic fracturing in permeable rocks. *Rock Mech Rock Eng* 37(4):251–275
- Zhu WC, Liu J, Yang TH, Sheng JC, Elsworth D (2006) Effects of local rock heterogeneities on the hydromechanics of fractured rocks using a digital-image-based technique. *Int J Rock Mech Min Sci* 43:1182–1199